# Electrical and thermal properties of bio-inspired laminated Cu/$Ti_3SiC_2$/C composites reinforced by graphene nanoplatelets

*Mu Wang[1,2], Xiaosong Jiang[1,2*], Hongliang Sun[1,2], Zixuan Wu[3], Liu Yang[4]*

*[1]Key Laboratory of Advanced Technologies of Materials, Ministry of Education, Chengdu 610031, China*

*[2]School of Materials Science and Engineering, Southwest Jiaotong University, Chengdu Sichuan 610031, China*

*[3]School of Engineering and Materials Science, Queen Mary University of London, London E1 4NS, United Kingdom*

*[4]Institute for Applied Materials (IAM-WK), Karlsruhe Institute of Technology (KIT), Karlsruhe 76131, Germany*

***Corresponding author**: xsjiang@swjtu.edu.cn **(X.S. Jiang)**

## Abstract

Taking inspiration from the unique hierarchical structure of bio-materials like pearl oyster, this study employs bio-inspired composites technological route using flake powder metallurgy to prepare laminated Cu/$Ti_3SiC_2$/C composites. The prepared composites have clear laminated structure, uniform dispersion of reinforcing phase and clean interface. At a Cu-plated GNPs content of 0.5 wt.%, the composites displayed tensile strength of 300.65 MPa, compressive strength of 575.32 MPa, electrical conductivity of 26.31 MS/m, and thermal conductivity of 285.87 $W \cdot m^{-1} \cdot K^{-1}$. The reinforcement of composites is caused by the load transfer effect of the laminated structure. During the loading process, the laminated structure creates multiple paths for deflecting cracks, which leads to the redistribution of the applied load. Moreover, the homogeneous distribution of GNPs throughout the laminated structure extends the mean free path of both free electrons and phonons within the material, consequently bolstering the electrical and thermal conductivity of the composites.

**Keywords**

Laminated structure, Mechanical properties, Electrical properties, Thermal properties.

## 1.Introduction

$Cu/Ti_3SiC_2/C$ composites demonstrate favorable mechanical and electrical properties, which can be attributed to the synergistic reinforcement achieved through the combined addition of multiple phases[1]. However, the agglomeration of reinforcing phases results in structural inhomogeneity of $Cu/Ti_3SiC_2/C$ composites. The comprehensive performance development of the composites is bottlenecked due to the inverse relationship between strength and toughness. Therefore, scholars have investigated various methods to achieve a real balance between strength and toughness. These methods mainly include: adding rare earth elements[2], introducing new reinforcing phases[3] or using large plastic deformations such as high-pressure torsion (HPT)[4]. These methods produced some results, but failed to achieve a balance between strength and toughness, resulting in poor overall performance.

Bio-materials like pearl oyster are characterized by simple composition, fine structure, and balanced strength and toughness[5]. The high strength and toughness of the material is attributed to its multi-component, multi-scale, multi-level composites "brick-mortar" layer structure[6, 7]. The laminated structure promotes harmonious structural and functional behavior by dissipating crack expansion energy through the effects of crack deflection, delayed necking, and stress-scattering waves[8]. This laminated structure, based on the principle of uniform dispersion of the reinforcing phase, has been applied to fine-tune the structure and properties of MMCs. The resulting materials exhibit superior strength and plasticity compared to conventional MMCs[9]. In addition, the laminated structure enhances the continuity of the highly thermally conductive and electrically conductive reinforcing phase, which contributes particularly to the thermal and electrical properties of carbon-reinforced Cu-matrix composites[10]. Thus, emulating the distinctive micro-structure present in pearl oysters could be a viable approach, and the application

of this "brick-mortar" laminated structure to Cu/$Ti_3SiC_2$/C composites has not been explored yet.

In laminated MMCs, the formation of "brick-mortar" laminates is accomplished by incorporating high-strength, high-aspect-ratio "bricks" paired with ductile metallic "mortars". Various methods, including flake powder metallurgy (FPM), vacuum filtration, and pre-molding[11, 12], are commonly utilized for manufacturing laminated composites. Among them, FPM is a simple and efficient method to enhance the geometrical compatibility with the 2D reinforcing phase by making thin slices of metal particles, and then constructing composites with uniformly dispersed reinforcing phases and well-defined laminated structures[13, 14]. Due to its excellent plasticity, the Cu matrix can fully utilize the toughening effect of the "mortar" in the Cu/$Ti_3SiC_2$/C composite system. Selecting the appropriate "bricks" is a challenging task that necessitates the incorporation of a material exhibiting high strength, Thermal conductivity (TC), and conductivity to regulate the composites overall performance. Graphene nanoplatelets (GNPs) exhibit exceptional mechanical, thermal, and electrical properties[15, 16]. Furthermore, GNPs can transfer high loads to enhance the strength of composites and improve their fracture toughness by providing crack bridging and deflection at heterogeneous interfaces[17]. Therefore, GNPs can serve as an optimal "brick" module in the Cu/$Ti_3SiC_2$/C composites system.

However, agglomeration of GNPs and mismatch at the interface between Cu and GNPs is another challenge[18, 19]. Building on prior research into Cu/$Ti_3SiC_2$/C composites, it has been demonstrated that modifying the surface of GNPs via an aqueous rutin solution is a straightforward and viable solution to mitigating agglomeration[1]. However, this method's dispersion effect is unstable and requires improvement. Based on the above methodology, it appears feasible to create transition phase between Cu and GNPs by chemically plating Cu onto the surface of GNPs (GNPs@Cu)[20, 21]. The Cu coating overcomes wettability and poor interface bonding, while maintaining the structural integrity of the GNPs. Additionally, it also improves the dispersion of GNPs in the Cu

matrix [22, 23]. The interface between GNPs and Cu, which is enhanced through Cu plating, eradicates the potential threats of interface defects.

Briefly, this study describes the preparation of flaky copper powders using FPM. A novel method combining physicochemical dispersion and chemical plating was used to mitigate the aggregation of graphite and GNPs. The Cu/$Ti_3SiC_2$/C/GNPs@Cu composites were then sintered by vacuum hot pressing (VHPs). A bionic laminated structure was successfully introduced into the Cu/$Ti_3SiC_2$/C composites, thus realizing an innovation in the structural design of this system. In this study, the effect of the laminated structure on the microstructure and properties of the composites was investigated. The laminated composites showed significant improvement in strength, ductility, electrical and thermal properties. This provides an effective method for the development of new composites with excellent overall performance.

## 2.Experiment

### 2.1.Raw materials

The matrix material was Cu powder (purity 99.99 %,300 mesh). The reinforcing phases were GNPs (purity 99.9 %, <10 layers), $Ti_3SiC_2$ (250 mesh), graphite (250 mesh). In this experiment, Cu was plated on the surface of graphite and GNPs using chemical plating. The aqueous rutin solution was utilized to immerse the GNPs for 15 min to enhance their dispersion initially. The surface of GNPs was roughened using a hydrochloric acid/ethanol solution. Under the conditions of stannous chloride sensitization and palladium chloride activation, copper-plated GNPs (GNPs@Cu) were prepared by adding GNPs to a heated copper-plating solution with stirring. Cu plated graphite (Gr@Cu) was obtained using the same procedure as GNPs@Cu.

### 2.2.Preparation of the laminated composites

This study involved the preparation of four laminated composites with varying GNPs@Cu contents. The $Ti_3SiC_2$ content was 10 wt.%, and Gr@Cu content was 3 wt.%. The GNPs@Cu contents were 0 wt.% (0.5 wt.% for GNPs), 0.5 wt.%, 1 wt.%, and 1.5 wt.%. Cu flakes were prepared by grinding spherical copper powder for 6 hours using

ethanol as a medium in a high-energy ball mill with the speed of 300 rpm and ball-to-powder ratio of 20:1). The raw materials were then proportionately weighed and mixed for 1 hour using a high-energy ball mill. The resulting slurry was dried using a vacuum freeze dryer (FD-A-50) for 24 hours. Subsequently, the composite powders were sintered and molded with VHPs at a sintering pressure of 30 MPa and a sintering temperature of 950 °C and cooled with the furnace. The preparation process is shown in Fig. 1.

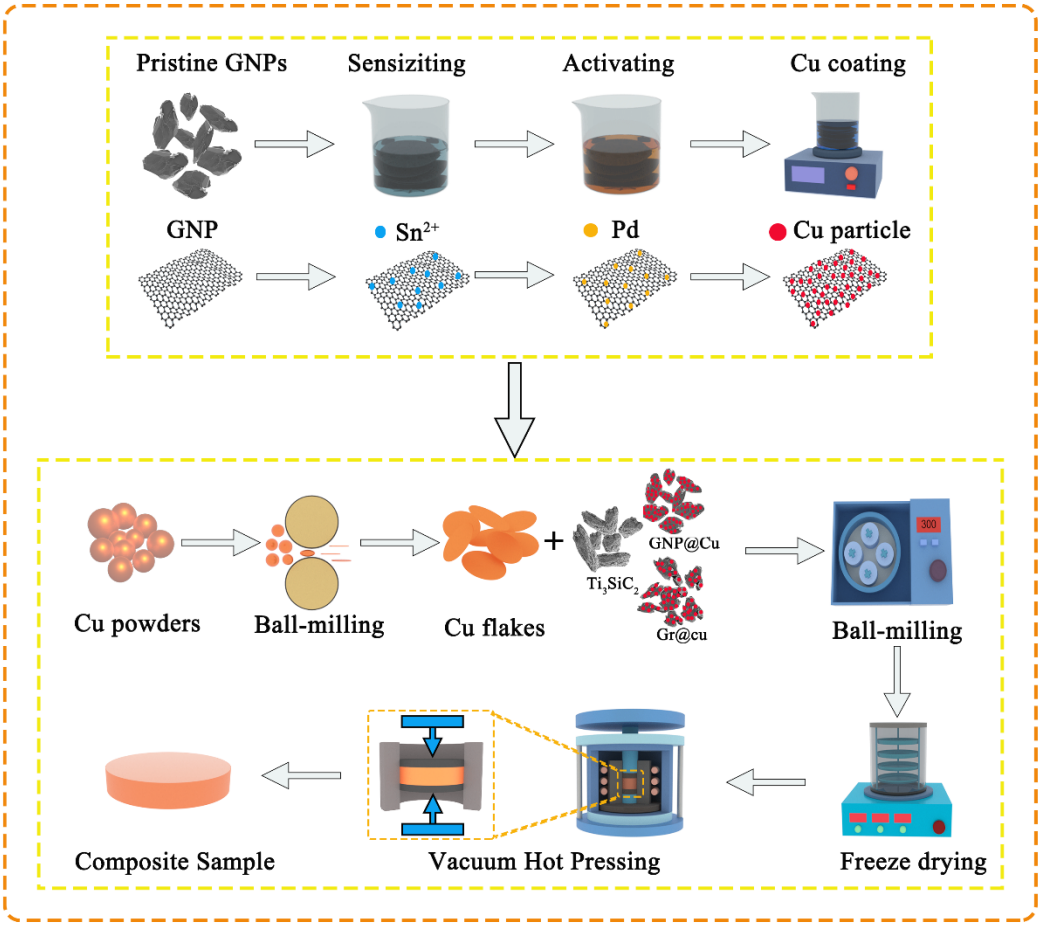


**Fig. 1.** Flowchart for the preparation of Cu/$Ti_3SiC_2$/C/GNPs@Cu laminated composites.

### 2.3.Characterization of the laminated composites

The density of the specimens is measured using Archimedes' principle, which in turn calculates their relative density. The microstructure and phase of the powders and samples were observed using scanning electron microscopy (SEM, ZEISS Sigma 300) and x-ray diffraction analysis (XRD, Rigaku XRD-6100). Transmission electron microscopy (TEM,

FEI Talos F200X) was used to further analyze the microstructure of the samples. The Microhardness tester (HXD-100TM/LCD) was utilized for measuring hardness. Composites' tensile and compressive strengths were measured using a universal testing machine (WDW-3100). Conductivity was measured using a resistivity tester (FT-300A1). Laser thermal conductivity instrument (NETZSCH LFA467) was used to measure the thermal diffusion coefficients of the composites in X-Y direction and Z direction.

## 3.Results and discussion

### 3.1.Microstructure of the powders

#### 3.1.1.Microstructure and formation mechanism of GNPs@Cu

As depicted in Fig. 2(a), the original GNPs tend to stack and agglomerate between the lamellae due to van der waals forces(VDW)[24], which leads to an increase in their folds. Fig. 2b show the GNPs with Cu particles of different sizes distributed on the surface (stirred for 5 min), but the deposition was incomplete due to the short time. After stirring for 10 minutes, the coverage area of Cu particles on the surface of GNPs significantly increased. However, some voids still remained unfilled by Cu particles (Fig. 2c). After 15 minutes of stirring, the surface of GNPs was coated with a dense, thin and uniform layer of Cu particles, yielding the best results (Fig. 2d). If the stirring time exceeded 15 minutes or the reaction was too aggressive, the Cu-plated layer thickened and was more prone to detachment.

Obviously, the plating effect is influenced by factors such as pre-dispersion, sensitization, activation effect, and plating solution environment. The pre-dispersion of rutin reduces the agglomeration of graphene flakes, facilitating adhesion of the subsequent plating layer to the monolayer GNPs and preventing multilayer adhesion. Luo et al. demonstrated that an excessive introduction of $H^+$ during sensitization and activation can impair the particle attachment environment on the surface of GNPs，which can lead to a non-uniform distribution of the plated layer[25]. Thus, in order to stabilize the reduction of Cu nanoparticles, $Cu^{2+}$ must be present in an alkaline environment at a

specific temperature. In addition, the formation mechanism of Gr@Cu is the same as that of GNPs@Cu[26].

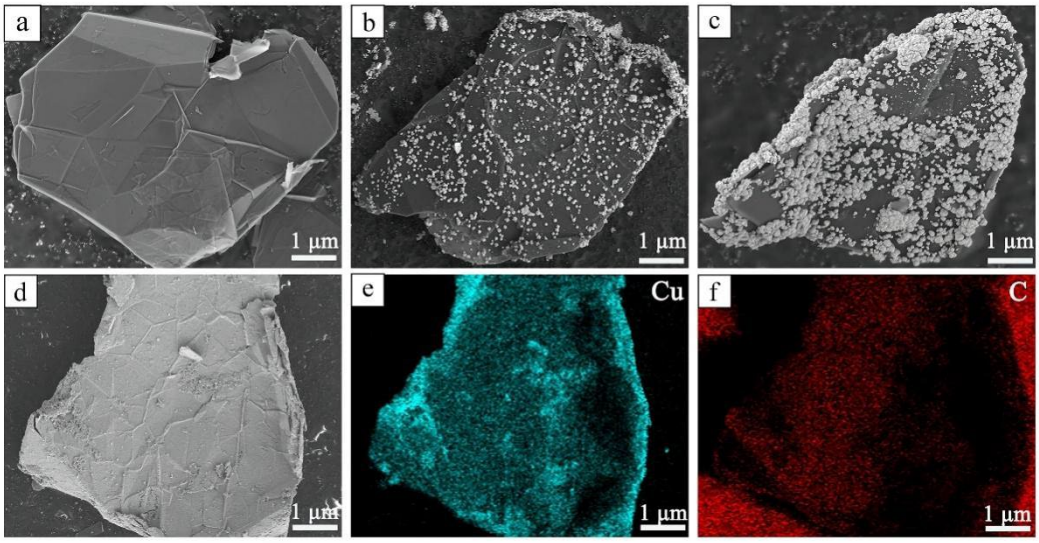


**Fig. 2.** SEM images: (a) original GNPs; (b) GNPs@Cu after agitation for 5 min, (c) GNPs@Cu after agitation for 10 min, (d) GNPs@Cu after agitation for 15 min, (e-f) the the element distribution in (d).

### 3.1.2.Microstructure of the composite powders

Based on Cu's good plasticity, high-energy ball milling was utilized to alter the morphology of the powder particles. As shown in Fig. 3(a), the Cu powder is presented in the form of uniform flakes after 6 hours of mechanical ball milling, with smaller Cu flakes adhering to the larger size Cu flakes. The transverse size of Cu flakes is distributed between 10 μm and 60 μm, while the longitudinal size is on the nanoscale. The significant transverse dimensions of the flake Cu powders minimize the count of interfaces, ultimately lowering the interface thermal resistance [27, 28].

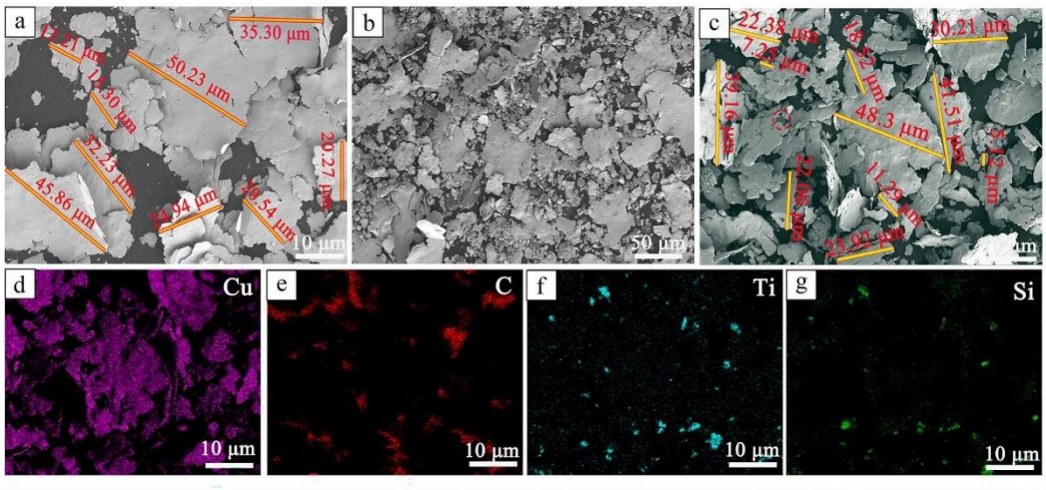


**Fig. 3.** SEM images of composite powders: (a) Cu powder ball milling for 6 hours, (b-c) composite powders mixing for 1.5 hours, (d-g) the element distribution maps in (c).

When the Cu flakes were mixed with other reinforcing phase powders in a ball milling tank for 1 hour, the flakes were disrupted into smaller particles with transverse sizes maintained in the range of 1 μm-50 μm, and the longitudinal sizes were significantly enlarged (Figs. 3b, 3c). Under the influence of ball milling, some of the graphite and GNPs were mechanically cold welded to Cu flakes. $Ti_3SiC_2$ was evenly distributed throughout the ball milling process and found in the composite powders as small particles. The composite powder EDS results are illustrated in Figs. 3(d-g), that ball milling reduces the powder particle size and boosts the opportunity for inter-powder contact, helpful for guaranteeing homogeneous dispersion of the reinforcing phase in the matrix.

### 3.2.Microstructure of laminated composites

#### 3.2.1.XRD analysis

Fig. 4 shows the XRD pattern of laminated composites. The XRD patterns of the sintered composites exhibited similarity to those of the composite powders. Upon comparing the XRD patterns of the composites before and after sintering, it is apparent that the characteristic peaks of Cu have shifted towards lower angles. The correlation between the crystal plane spacing and the angle of diffraction may be deduced using the Bragg diffraction equation[4]:

$$2dSin\theta = n\lambda \quad (1)$$

Where d is the crystal plane spacing, θ is the diffraction angle, λ is the wavelength, and n is a constant. As the θ decreases, the d increases, indicating a distorted lattice of Cu. Furthermore, the intensity and width of the copper peaks varied with the increase in GNPs@Cu content, and this variation was associated with the grain structure. To analyze this variation, we calculated the crystal size using the William-Hall equation[29, 30]:

$$D = \frac{0.9\lambda}{BCos\theta} \quad (2)$$

where D is the grain size, B is the full width at half maximum (FWHM), λ is the wavelength, and θ is the peak position. The average grain sizes of the composite powders and the four composites were 531.26 nm (powders), 472.68 nm (0.5 wt% GNPs), 467.21 nm (0.5 wt% GNPs@Cu), 442.26 nm (1.0 wt% GNPs@Cu), and 453.24 nm (1.5 wt% GNPs@Cu) . The smaller grain size after sintering is attributed to the work hardening of the copper flakes caused by the ball milling process, which leads to recrystallization refinement during VHPs. As the content of GNPs on Cu increases, the grain size decreases. This is because the high specific surface area of GNPs provides nucleation sites for the formation of new grains during the sintering process, which hinders grain growth and leads to grain size refinement[31] . However, when the content of GNPs exceeded 1.0 wt%, the grain size of the composites increased instead. This may be because the GNPs exceed the optimum threshold for effective grain refinement and agglomeration of GNPs begins to dominate. This agglomeration prevents uniform distribution of strain during processing, resulting in a reduction in the effectiveness of grain boundary pinning and coarsening of grains in localized regions.

The composite powder's XRD pattern displayed a marked $Ti_3SiC_2$ characteristic peak close to a diffraction angle of 39.581°, while the intensity of said peak reduced in the composites sample after sintering. The peaks that characterize TiC were identified at 41.710° and 35.906°. Around the diffraction angle linked to the characteristic peak of Cu (111), the $Cu_9Si$ was detected. This denotes the reaction between Cu and $Ti_3SiC_2$ during

the sintering procedure and the formation of a new phase[1]. The subsequent analysis of the TEM results will focus on the reaction between Cu and $Ti_3SiC_2$.

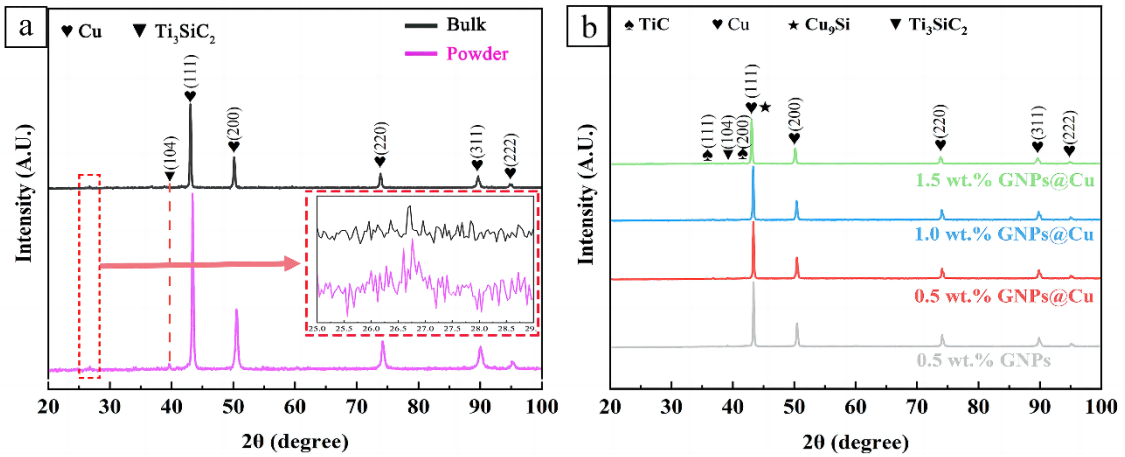


**Fig. 4.** XRD patterns of laminated composites:(a) powders and bulk, (b) composites with different GNPs@Cu contents.

### 3.2.2.Microstructure of the laminated composites

The cross-sectional microscopic morphology of the laminated composites is shown in Fig. 5 (a-e). The gray-white region is the Cu matrix, the gray particles are $Ti_3SiC_2$ and TiC phases, and graphite is a long curved black strip. The small particles of GNPs are uniformly distributed between the "brick" module and the "mortar" module. The formation of the laminated structure in Cu-based composites is influenced by several factors, such as cold welding through ball milling , gravitational self-assembly of powders , and particle sliding and rearrangement during sintering[11]. During the procedure of introducing the evenly combined composite powders into the VHPs mold, consistent shaking permits the flake powder to be arranged in a systematic direction under the pull of gravity. The laminate Cu powder and the two-dimensional reinforcing phase have a tendency to align at a specific angle[32]. The sintering process had an impact on the development of the laminated structure. During sintering, the Cu flakes in a semi-molten state undergo stacking and rearrangement under pressure. This outcome leads to a gradual filling of the gap between the Cu particles and the reinforcing phase. Under longitudinal pressure, semi-molten Cu flows transversely and generates transverse plastic deformation.

The graphite and GNPs experience compression due to the surrounding Cu matrix, causing distribution in a direction perpendicular to the pressure. Eventually, the Cu flakes bonded and diffused, resulting in a laminated structure resembling a pearl shell. As shown in Fig. 5 (f-i), there is no gap between the interfaces.

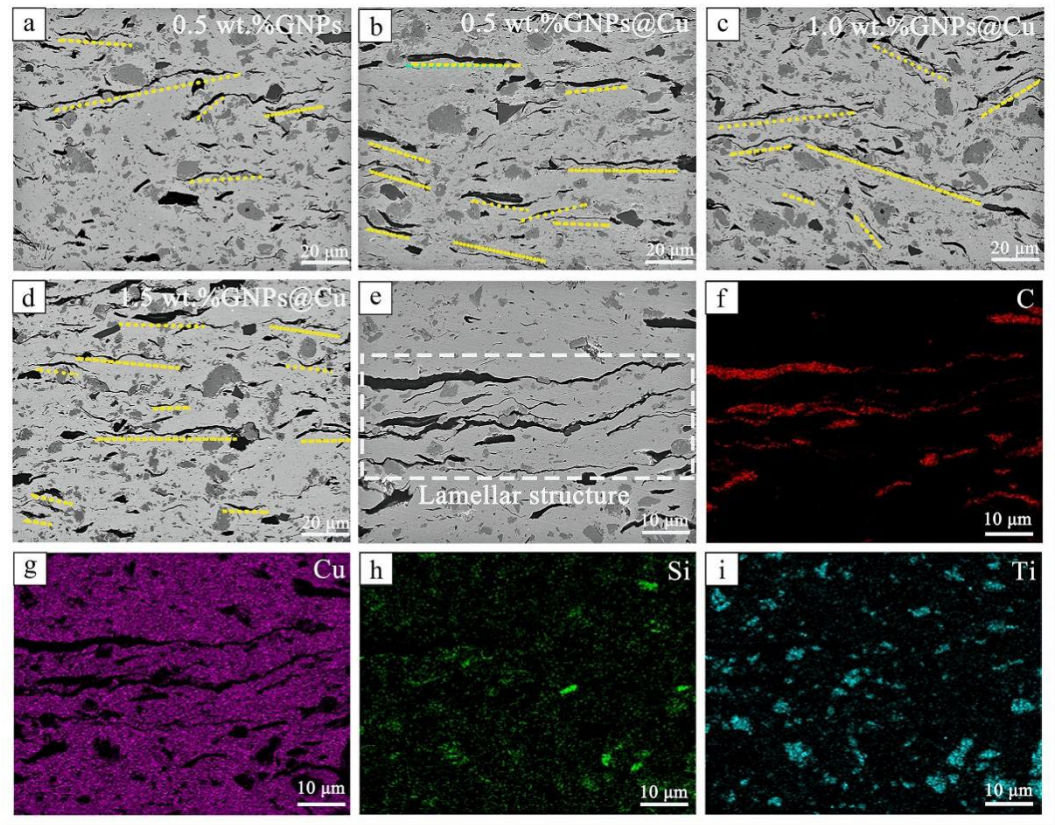


**Fig. 5.** SEM images of the cross-section (X-Y direction) of the laminated composites: (a) 0.5 wt.% GNPs, (b-c) GNPs@Cu 0.5 wt.%, 1.0 wt.%, 1.5 wt.%, (e-i) laminated structure.

### 3.2.3.Interface reactions and structure

The interface structure of the reinforcement and matrix can be observed and analyzed at the microcosmic level by using TEM. Fig. 6(a) displays the dark field TEM image of laminated composites containing 0.5 wt.% GNPs@Cu. The Cu matrix is off-white, $Ti_3SiC_2$ appears dark grey, and GNPs are bright white. Fig. 6(b-d) displays the elemental distribution of Cu, C, Ti, and Si, where the interface between $Ti_3SiC_2$ and the Cu matrix is tightly coupled and without an obvious boundary. As illustrated in Fig. 7, the

interface between the substrate and GNPs is flawlessly bonded and devoid of impurities. Despite the non-wettability of Cu and GNPs, their interface remains continuous and immaculate without any gaps (Fig.7b). This phenomenon is attributed to the mechanical interlocking between the Cu coating and GNPs, as well as the metallurgical fusion of the Cu coating to the Cu substrate. A significant distinction in morphology between the Cu coating and substrate was observed. This can be ascribed to the weaker crystallinity of the Cu coating in comparison to that of the Cu substrate under alternating hot and cold stresses[33].

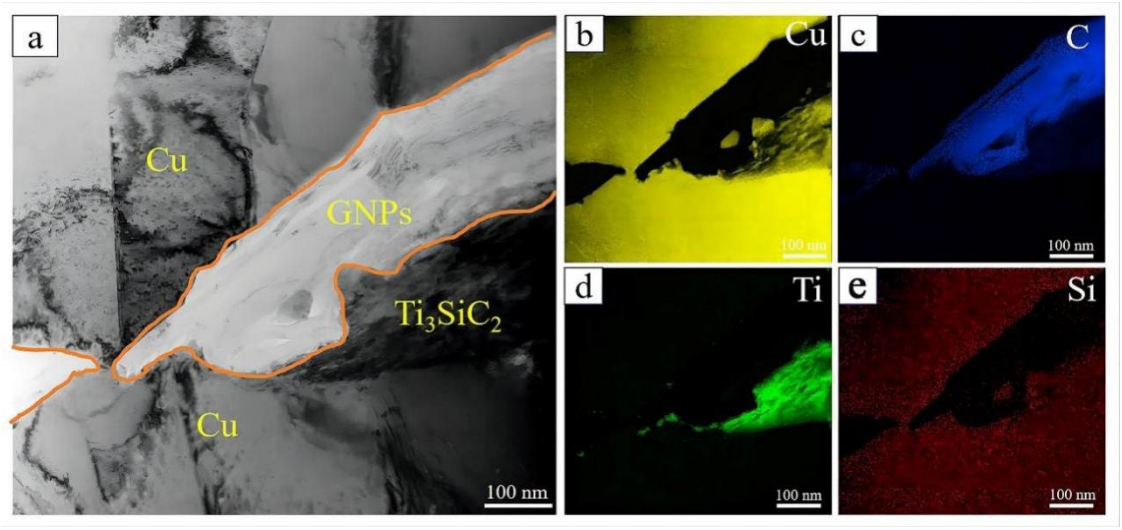


**Fig. 6.** TEM images of 0.5 wt.%GNPs@Cu laminated composites:(a) Interfaces of composite materials; (b-f) Elemental distributions.

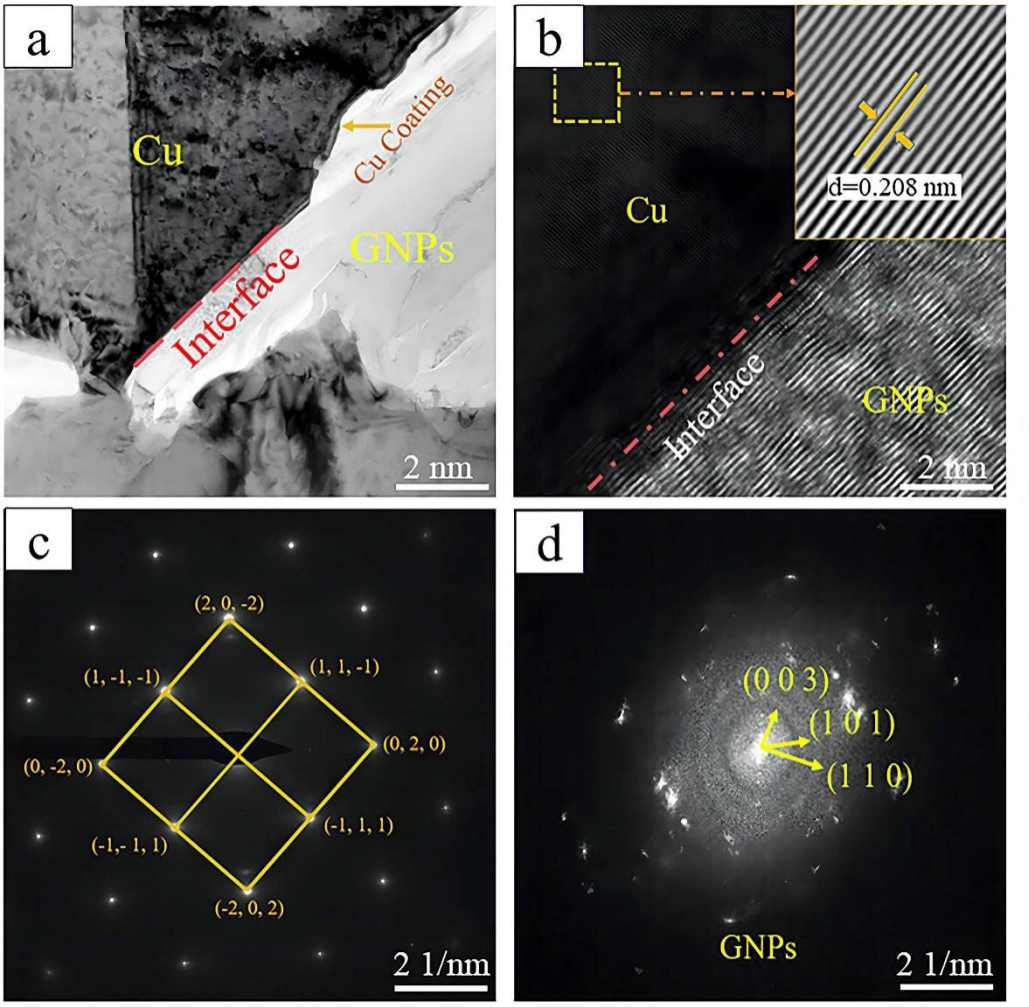


**Fig. 7.** TEM image of 0.5 wt.%GNPs@Cu laminated composites: (a) Interfaces between Cu and GNPs, (b) HRTEM image of the interface, (c) diffraction pattern of Cu, (d) diffraction pattern of GNPs.

It has been demonstrated that the wettability of metals and ceramics is contingent on the interface interaction between them, and the favorable wettability of Cu and $Ti_3SiC_2$ arises from their interface reaction[34]. As shown in Fig. 8, the $Ti_3SiC_2$ and Cu matrices are tightly bonded to each other and there is no clear boundary. However, a tissue made of bright white and grey slats is visible at the interface's edge. Based on EDS data, it is evident that the grey slats contain a Cu matrix, the bright white slats' primary composition is TiC, containing a small quantity of $Ti_3SiC_2$. Fig. 9 shows a high-resolution image of the TiC and Cu interface, where TiC and Cu are interspersed with each other to form a nanoscale laminated structure and overlap in some regions with a clean and continuous

interface. Thermal decomposition of $Ti_3SiC_2$ at sintering temperature of 950°C has been demonstrated[35]. $Ti_3SiC_2$ crystals exhibit robust Ti-C bonding and comparatively weak Ti-Si bonding[36]. Due to thermal activation, a small quantity of Si was de-embedded and diffuses from $Ti_3SiC_2$ into Cu to create solid solutions or intermetallic compounds. As Si diffuses outwards and volumes of $Ti_3SiC_2$ contract, Cu diffuses into $Ti_3SiC_2$ along the contraction direction. Ultimately, $Ti_3SiC_2$ near Cu gets converted to TiC due to Si escaping. This was described the interdiffusion and phase transition between Cu and $Ti_3SiC_2$[28]. The final interface products were confirmed to be mainly TiC and $Cu_9Si$, which was done through the use of chemical equations combined with Gibbs free energy changes[29].

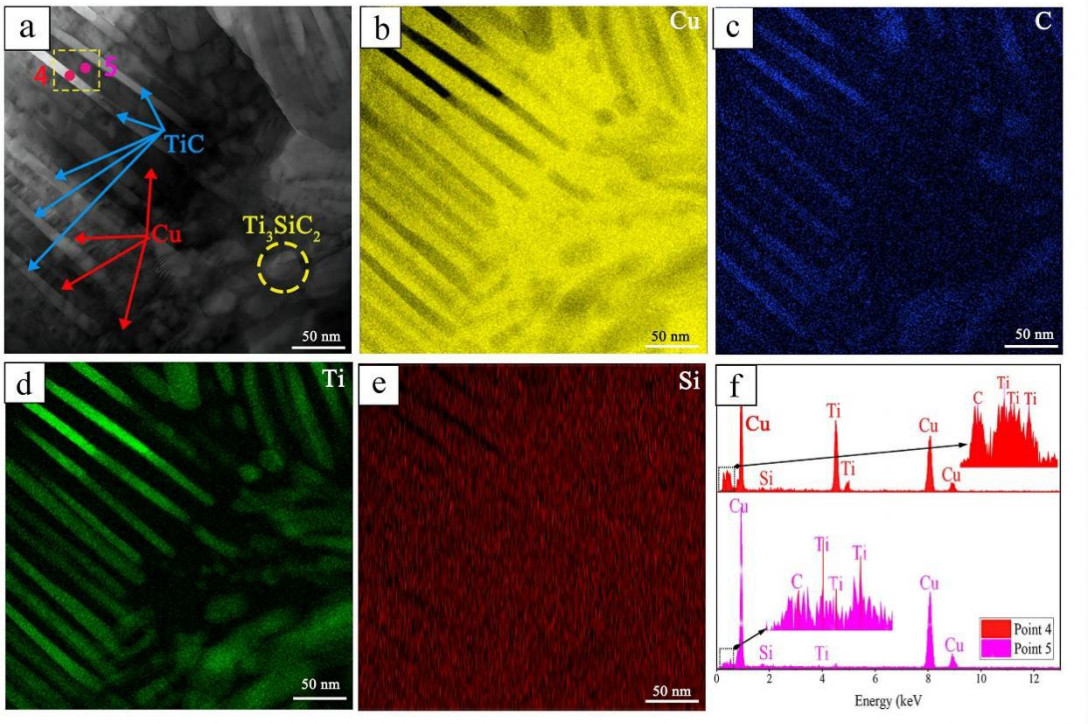


**Fig. 8.** TEM images of 0.5 wt.%GNPs@Cu laminated composites:(a) Interfaces of composite materials, (b-e) elemental distributions, (f) EDS patterns of Point 4 and Point 5.

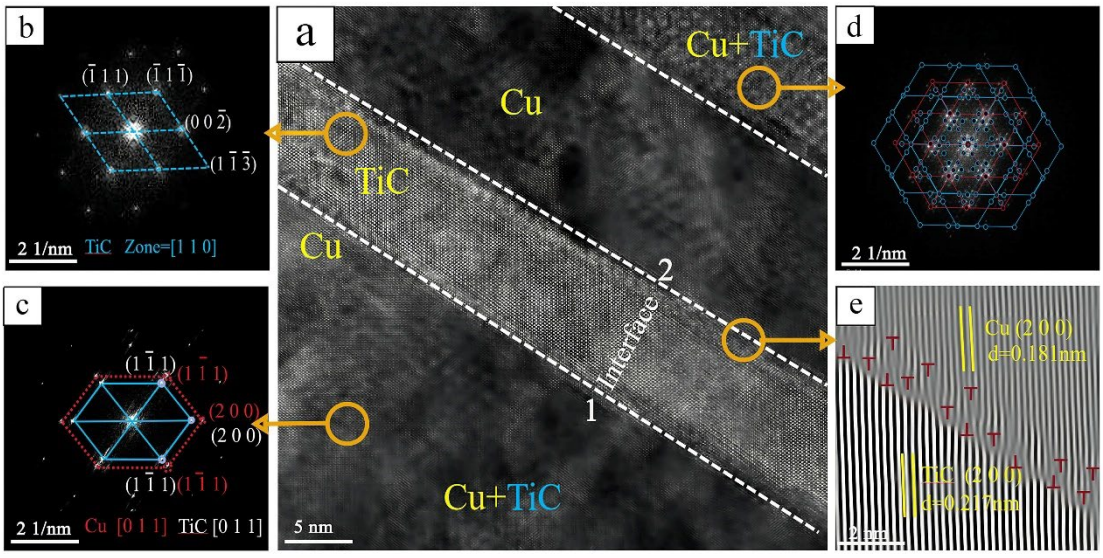


**Fig. 9.** TEM images of 0.5 wt.%GNPs@Cu laminated composites: (a) HRTEM image of the interface, (b) the diffraction pattern of TiC, (c, d) the diffraction pattern of Cu and TiC, (e) the dislocation distribution at the interface.

### 3.3.Performances of the laminated composites

#### 3.3.1.Mechanical performance

The composites containing 0.5 wt.% GNPs@Cu exhibited the highest microhardness (145.3 HV) and relative density (98.85%), as depicted in Fig. 11(a). The density and hardness of the 0.5 wt.% GNPs@Cu sample has increased, which can be attributed to the improved interfacial bonding between the reinforcing phase carbon material and the Cu matrix due to the coating. However, the relative density and hardness gradually decreased with the increase of GNPs@Cu content. As demonstrated in Fig. 10(b, c), the addition of 0.5 wt.% GNPs@Cu resulted in an increase in the tensile strength, compressive strength, elongation, and shrinkage of the composites, reaching 300.65 MPa, 575.32 MPa, 7.85%, and 27.3%. The mechanical properties of the specimens exhibited a declining trend as the content of GNPs@Cu increased. Furthermore, the mechanical characteristics of Cu/$Ti_3SiC_2$/C composites, previously documented in literature, are outlined and contrasted (Fig. 10(d,e)). When comparing with the conventional structure,

the use of a laminated structure yields a noteworthy enhancement in the tensile strength, compressive strength and toughness of the composites.

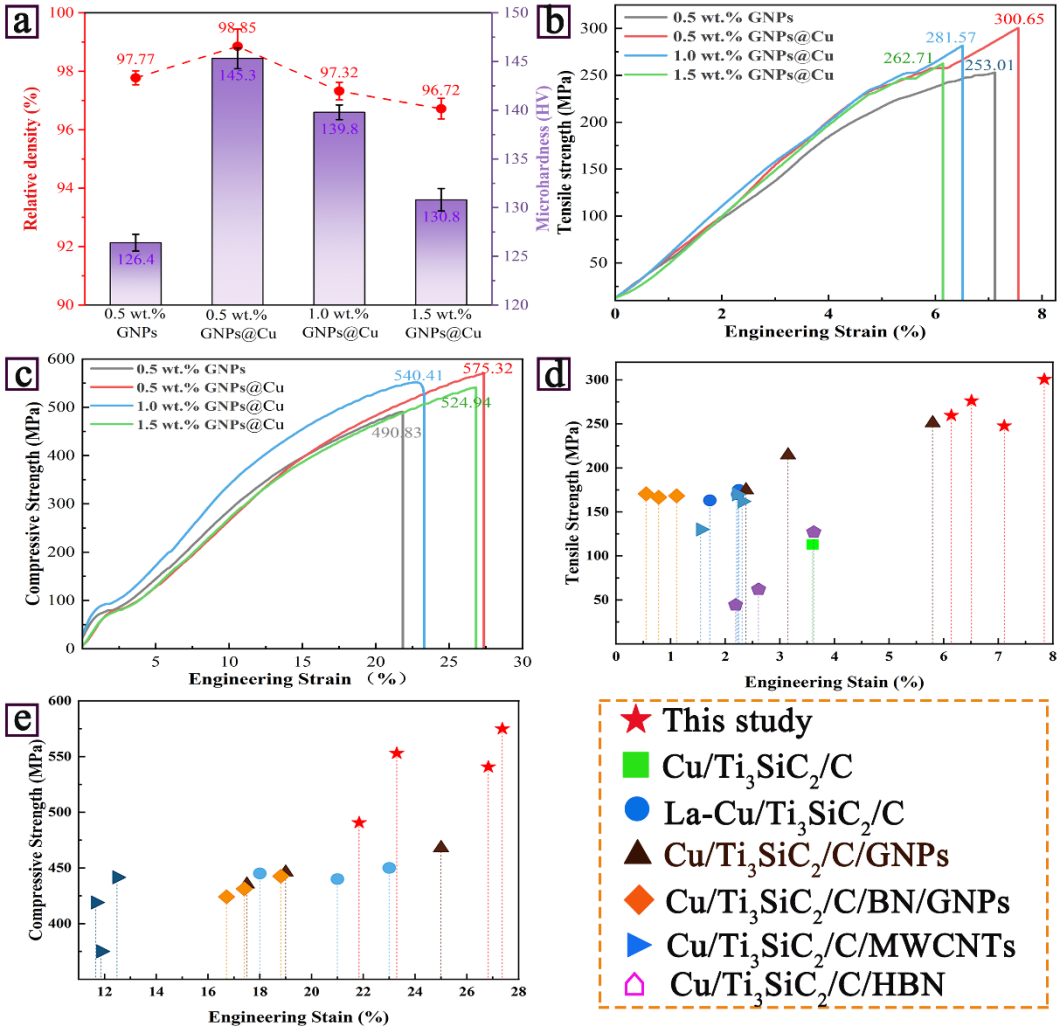


**Fig. 10.** (a) microhardness and relative density; (b) tensile strength, (c) compressive strength, (d) comparison of tensile strength data, (e) comparison of compressive strength data[1, 4, 37, 38].

As shown in Fig.11, the phase distribution at the tensile fracture of 0.5 wt.%GNPs@Cu composite material is uniform, and the laminated structure is obvious. Furthermore, dimples are consistently distributed throughout the fracture indicating the material's good ductility. Graphite and GNPs are regularly distributed among the Cu layers in the planar direction, forming a stacked structure with Cu that exhibits good interface bonding (Fig. 11b). Obvious pores resulting from the pull-out of the GNPs are

observed, suggesting that a certain percentage of the load is transferred to the GNPs under the external force, resulting in the pull-out of the GNPs. GNPs exhibit high load-bearing properties in laminated composites, when composites undergo external tensile stresses, the matrix loads are predominantly shared through the transfer of interface stresses[39].

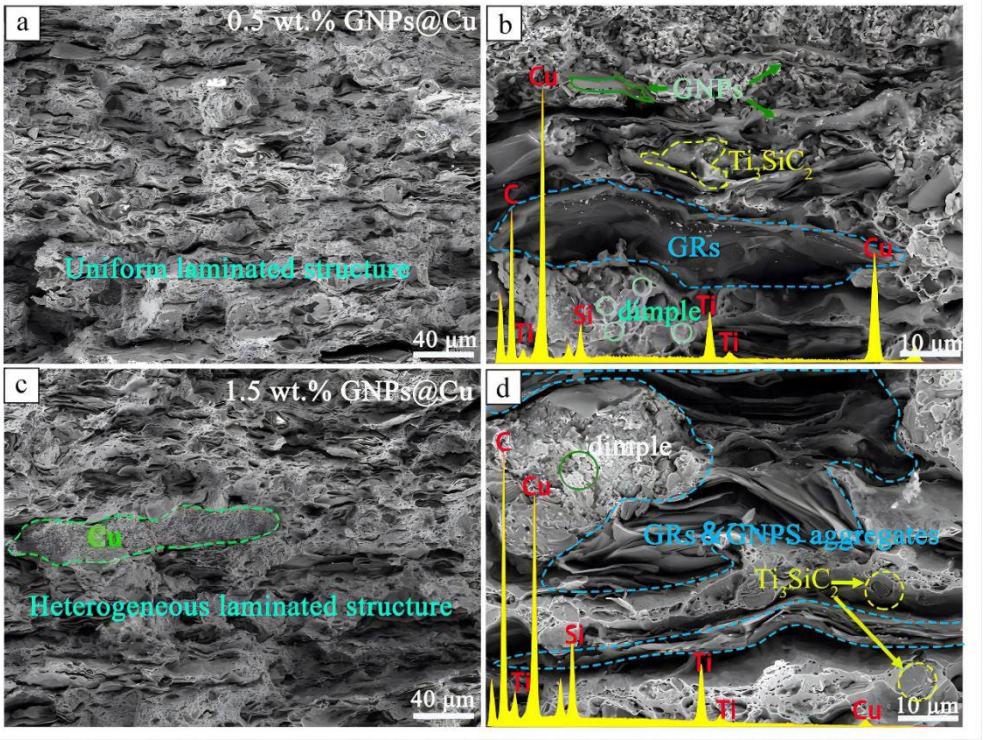


**Fig. 11.** SEM images of tensile fracture of laminated composites: (a) GNPs@Cu 0.5 wt.%, (b) local magnifications of (a), (c) GNPs@Cu 1.5 wt.%, (d) local magnifications of (c).

The GNPs' load transfer enhancement effect depends on the volume fraction and effective aspect ratio of GNPs, as proposed by the shear hysteresis theoretical model[1, 40]. Increasing the volume fraction and transverse dimension of GNPs have a positive influence on the composites' yield strength. However, graphite and GNPs are attracted to each other through VDW, and their tendency to clump together increases with higher concentration. As illustrated in Fig. 11(c, d), the fracture of the 1.5 wt.% GNPs@Cu composites reveals distinct regions enriched in Cu. This is attributable to a large number of pores arising from the aggregation of Gr and GNPs, which results in the uneven distribution of phases. Furthermore, the microscopic defects generated by agglomerated

GNPs hinder dislocation motion, leading to dislocation build-up and stress concentration. The reinforcing phase and the matrix possess different deformation capacities resulting in uncoordinated deformation, then the elongation of the composite material is reduced[17].

To further explore the toughening mechanism of composites through "brick" and "mortar" modules within laminated structures, this paper introduces a failure model based on shear hysteresis theory [41]:

$$S_C = {}^{\sigma_p}/_{\tau_y} \quad (3)$$

Where the critical aspect ratio of the "brick" module is $S_C$, the tensile strength of the "brick" module is $\sigma_p$, and the yield shear strength of the "mortar" module is $\tau_y$. There are two failure modes present in GNPs-reinforced laminated composites[26]. If the brick aspect ratio ($S_r$) is higher than the critical aspect ratio ($S_r > S_C$), the composites demonstrates a failure mode of reinforced-phase fracture, which indicates a brittle material. If the brick aspect ratio is lower than the critical aspect ratio ($S_r < S_C$), the composites displays a failure mode of reinforced phase pull-out, indicating good ductility. The tensile strength of GNPs is 130 GPa, while Cu's shear strength ranges from 150-230 MPa [15]. Using these values, it can be estimated the critical aspect ratio of the "brick" module GNPs to be between 500-900. The multilayer GNPs utilized in this investigation had their longitudinal dimensions below 50 nm and transverse dimensions ranging from 10-25 μm ascertained through SEM and TEM. The range of the GNPs' actual aspect ratio $S_r$ encompasses the calculated critical aspect ratio $S_C$. Hence, the enhanced-phase fracture failure method and the enhanced-phase pull-out failure mode collaborate, and the illustration of the two failure modes working together is presented in Fig. 12. When composites are subjected to external forces, the loads are transferred from the matrix to the GNPs, and the unique folded structure of the GNPs has a tendency to unfold under directional loads, and this unfolding requires the absorption of energy, thus dissipating some of the loads. When external forces increase, GNPs with a smaller length-to-diameter ratio ($S_r < S_C$) or GNPs with lower bonding to the substrate, will be pulled out of the

substrate. GNPs with large aspect ratios ($S_r > S_C$) or in regions of stress concentration are prone to fracture. The pull-out mode enhances the toughness, whereas the fracture mode enhances the strength. Both modes work together to achieve a balanced combination of strength and toughness in laminated composites.

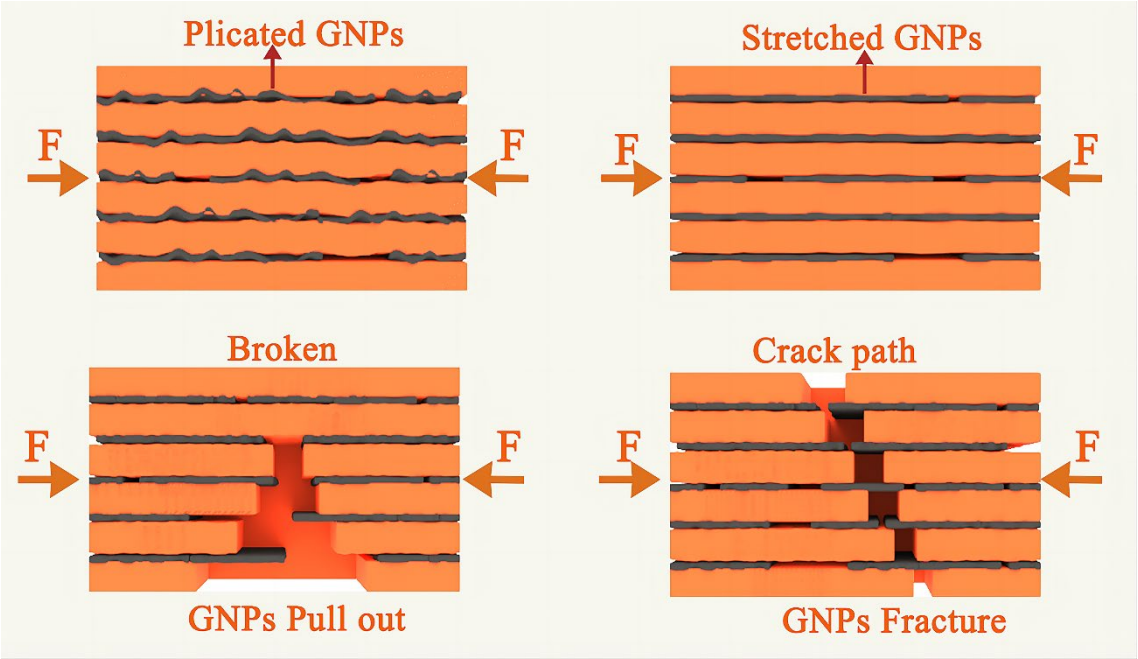


**Fig. 12.** Schematic diagram of the strengthening and toughening mechanism of laminated composites.

In addition to load transfer and dissipation mechanisms, grain refinement also affects the mechanical properties of composites. The effect of grain size on the properties of composites can be described by Hall-Petch's formula[42]:

$$\sigma_y = \sigma_0 + kd^{-1/2} \quad (4)$$

where: $\sigma_y$ is the yield strength of the material; $\sigma_0$ is the frictional stress of the material; k is the Hall-Petch constant; d is the average grain size. Both fine grains and derived more grain boundaries are able to act as barriers to dislocation movement, increasing the stress required for dislocations to pass through, thus increasing the yield strength and hardness of the material[43, 44]. From the XRD results it can be seen that grain refinement has a positive effect on the composite properties at GNPs contents of 0.5 wt% and 1.0 wt%, but refinement is hindered at GNPs content of 1.5 wt%, at which point the contribution of the

fine grain strengthening mechanism decreases. Therefore, the mechanical properties of composites are mainly influenced by mechanisms such as load transfer and grain refinement, which in turn are equally influenced by various factors such as interfacial bond strength, GNPs size and distribution, and matrix structural defects.

### 3.3.2.Electrical performance

As depicted in Fig. 13, the 0.5 wt.% GNPs@Cu composites exhibited the highest conductivity with a value of 26.32 MS/m. As the content of GNPs@Cu increases, however, the conductivity values decrease due to the increase in porosity and agglomerate content. The mobility of free charges in nanolaminated composites is intricately linked to their microstructure[45]. The continuity and uniform distribution greatly affect the conduction efficiency of both Cu network structures and laminated structures. Due to interface reactions, there is a small quantity of Cu (Si) solid solution present within the composites. The size and number of Si solute atoms have a certain effect on conductivity. The creation of a solid solution results in the distortion of Cu crystals and this increase in deformation leads to a rise in electron scattering and impedes free electron transfer. The TiC interface reaction product precipitates as a secondary phase, scattering electrons. Furthermore, the composites contain microscopic defects caused by phenomena such as interface reactions, reinforcing phase agglomeration, and grain refinement [46]. Hence, the conductivity of composites may be influenced by a plethora of factors working in combination. However, the conductivity values of the samples corresponded to their density and hardness, with the highest conductivity values observed when the density and hardness were at their maximum. The findings suggest that the conductivity of the laminated composites analyzed in this study is predominantly influenced by porosity and microscopic anomalies, including dislocations, grain boundaries and vacancies.

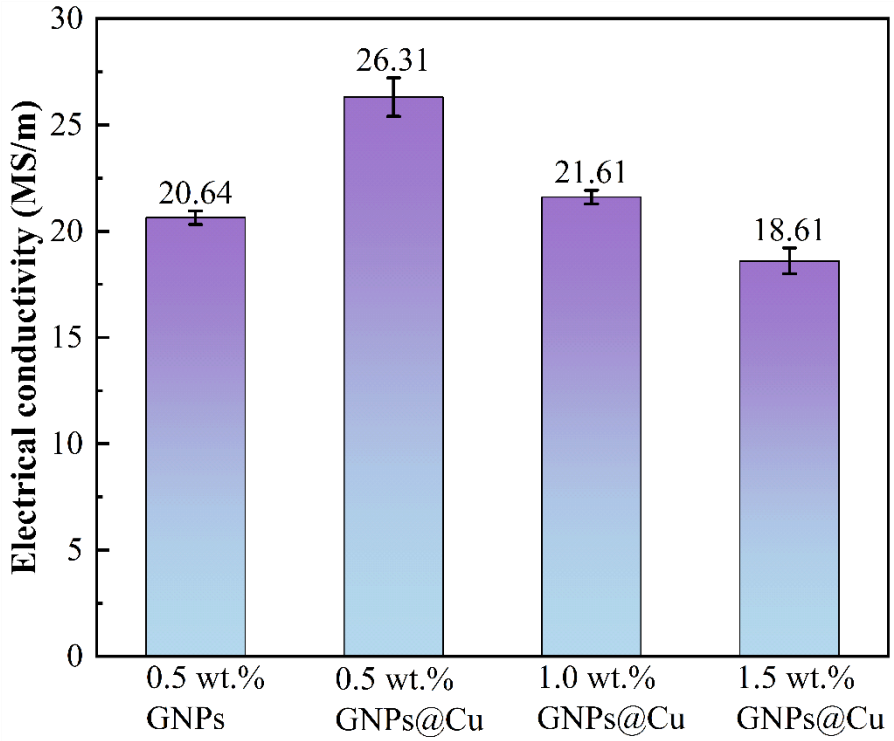


**Fig. 13.** Conductivity of laminated composites in the X-Y direction.

### 3.3.3.Thermal performance

The TC of GNPs in the in-plane direction exceeds that in the out-of-plane direction. Consequently, GNPs reinforced laminated composites' TC exhibits anisotropy [10]. The TC is determined by measuring the thermal diffusion coefficient α in various orientations of the composites and then applying the TC equation:

$$k = \alpha \cdot \rho \cdot C_P \quad (5)$$

Where k is TC ($W \cdot m^{-1} \cdot K^{-1}$), α is the thermal diffusion coefficient ($m^2/s$), ρ is density ($kg/m^3$), $C_P$ is specific heat capacity ($J \cdot kg^{-1} \cdot K^{-1}$)[47]. The specific heat capacity of laminated composites can be estimated from the linear law of mixtures[48]:

$$C_P = \sum Vol_{mi} C_p^i \quad (6)$$

Where $C_P$ denotes the specific heat capacity of the prepared composites, while $Vol_{mi}$ and $C_p^i$ represent the volume fraction and specific heat capacity of each phase of the composites.

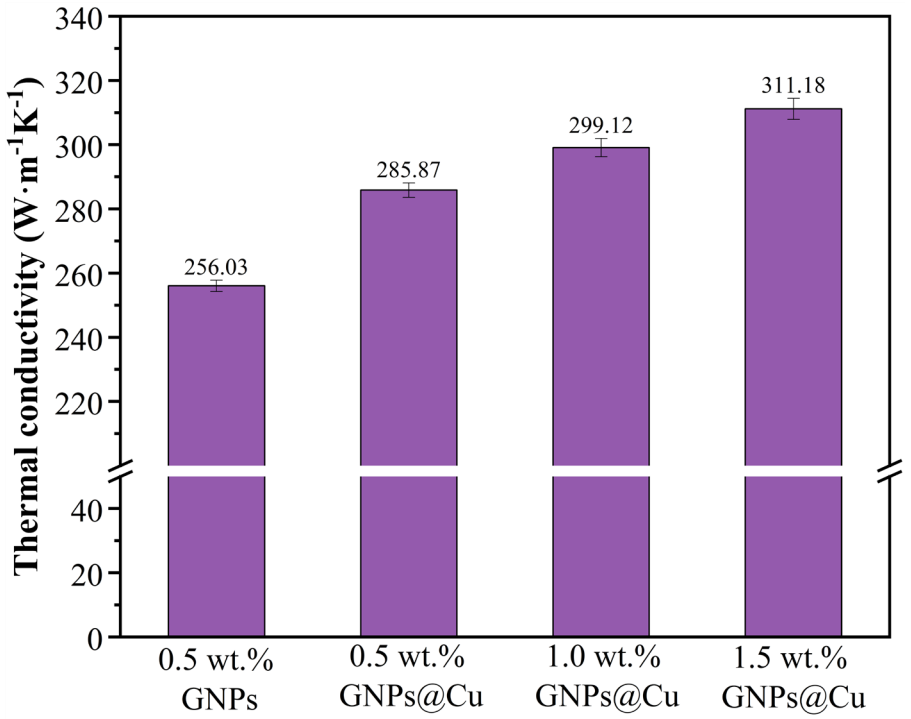


**Fig. 14.** Thermal conductivity of laminated composites in the X-Y and Z directions.

Fig. 14 displays the TC of four laminated composites with varying GNPs@Cu contents in the X-Y and Z directions. At a constant content level of 0.5 wt.%, the TC of the GNPs@Cu reinforced composites shows a substantial enhancement in comparison to the GNPs-reinforced composites. The Fig. indicates that the TC of the laminated composites in the X-Y direction amplifies as the GNPs content grows. In addition to the excellent TC of GNPs itself, the increase in GNPs content promotes the continuity of the laminate structure. On the contrary, the TC in the out-of-plane (Z) direction decreases with the increase of GNP content in the laminated composites. While the laminated structure proves effective in enhancing the TC of composites, the resulting enhancement faces a limitation due to thermal resistance at the solid-solid interface stemming from inherent vibrational mismatches[49]. The contact between graphite, GNPs and Cu matrix forms a discontinuous interface and the lattice defects such as dislocations and grain boundaries at the interface become the scattering centers of electrons and phonons, limiting the mean free range of electrons and phonons, which in turn reduces the TC of the composites [50]. Furthermore, the agglomeration of Gr and GNPs inevitably decreases

the bonding among Cu grains, augmenting porosity and resulting in the disturbance of the formation of thermal conductivity paths.

Additionally, the TC of GNP composites is influenced by the structural characteristics of the reinforcing phase, including defects, aspect ratios, and orientation[51]. Process of ball milling introduces structural defects in the GNPs. Consequently, these defects hinder the strong phonon scattering and ultimately weaken the intrinsic TC of the GNPs[52]. In addition, the aspect ratio and orientation of the GNPs are crucial factors. The GNPs utilized in this investigation have a lengthwise magnitude of 20-100 nm and a widthwise magnitude of 15-25 μm, classifying them as small-sized GNPs. Smaller-sized GNPs create greater GNP/Cu interfaces. Additionally, the small-sized GNPs exhibit random dispersion throughout the Cu matrix, rather than alignment in a singular direction, which impedes the GNPs' effective contribution to TC. When the GNPs are predominantly dispersed in the direction of heat flow (X-Y direction), and their plane aligns with the heat flow, the GNPs exhibit more significant thermal conductivity enhancement efficiency. In the direction perpendicular to the heat flux direction (Z direction), the contact area of GNPs with the matrix material is minimized and the number of effective thermal conductivity paths is reduced [10]. This ultimately indicates that GNPs reinforced laminated composites possess significantly anisotropic TC.

## 4.Conclusions

This study examines the microstructure and properties of Cu/$Ti_3SiC_2$/C bionic laminates that have been enhanced with copper-coated interfacial bonded GNPs prepared by FPM and VHPs. The prepared composites have an overall improved overall performance, which provides a potential option for the requirements of pantograph and other related applications. The key findings are as follows:

(1)The study found that the coating facilitates the transformation of the carbon material and copper matrix from mechanical bonding to mechanical-metallurgical bonding. This improves the interfacial bonding strength and promotes load transfer while reducing the interfacial thermal resistance.

(2) The composite material exhibits the best overall performance when the amount of GNPs@Cu is 0.5 wt.%. The material's hardness, tensile strength, elongation, compressive strength, electrical conductivity, and thermal conductivity were measured at 145.3 HV, 300.65 MPa, 7.845%, 575.32 MPa, 26.31 MS/m, and 285.87 $W \cdot m^{-1} \cdot K^{-1}$.

(3) The composites displayed a range of strengthening mechanisms, including load consumption and transfer mechanisms of GNPs and laminated structures, grain refinement, and second-phase strengthening. Additionally, coatings and laminated structures optimized the interfacial structure, reduced phonon scattering, and improved the planar electrical and thermal conductivity of the composites.

## Conflict of interest

The authors declare that they have no conflict of interest.


## Acknowledgments

This work was supported by Key Laboratory of Infrared Imaging Materials and Detectors, Shanghai Institute of Technical Physics, Chinese Academy of Sciences (No. IIMDKFJJ-21-10). We would like to thank Analytical and Testing Center of Southwest Jiaotong University for partial testing.


## Data Availability statement

The data used to support the findings of this study are available from the corresponding author upon request.

## References


[1] Jiang X, Liu W, Li Y, Shao Z, Luo Z, Zhu D, et al. Microstructures and mechanical properties of Cu/$Ti_3SiC_2$/C/graphene nanocomposites prepared by vacuum hot-pressing sintering and hot isostatic pressing. Composites Part B: Engineering. 2018;141:203-13.https://doi.org/10.1016/j.compositesb.2017.12.050

[2] Lv L, Jiang X-S, Zhang M-M, Sun H-L, Shao Z-Y, Fu N-N, et al. Effect of La on microstructures and mechanical properties of Cu/$Ti_3SiC_2$/C nanocomposites sintered by vacuum hot-pressing and hot isostatic pressing. Materials Research Express. 2020;7.https://doi.org/10.1088/2053-1591/ab5df6

[3] Shu R, Jiang X, Liu W, Shao Z, Song T, Luo Z. Synergetic effect of nano-carbon and HBN on microstructure and mechanical properties of Cu/$Ti_3SiC_2$/C nanocomposites. Materials Science and Engineering: A. 2019;755:128-37.https://doi.org/10.1016/j.msea.2019.04.002

[4] Wu Z, Jiang X, Li Y, Christian P, Sun H, Zhang Y, et al. Microstructures and properties of graphene nanoplatelets reinforced Cu/$Ti_3SiC_2$/C nanocomposites with efficient dispersion and strengthening

achieved by high-pressure torsion. Materials Characterization. 2022;193:112308.https://doi.org/10.1016/j.matchar.2022.112308
[5] Meyers MA, McKittrick J, Chen P-Y. Structural biological materials: critical mechanics-materials connections. Science. 2013;339:773-9.https://doi.org/10.1126/science.1220854
[6] Wegst UG, Bai H, Saiz E, Tomsia AP, Ritchie RO. Bioinspired structural materials. Nat Mater. 2015;14:23-36.https://doi.org/10.1038/nmat4089
[7] Fouly A, Kuppusamy S, Kulandaivel A, Abdullaev S, Fathy A, Hassan A, et al. Design and high efficient construction of bilayer $NiCoO_2$/Poly(1-NA-co-oT) nanocomposite absorber for X-band stealth applications. Vacuum. 2024;220.https://doi.org/10.1016/j.vacuum.2023.112792
[8] Wu H, Fan G, Huang M, Geng L, Cui X, Xie H. Deformation behavior of brittle/ductile multilayered composites under interface constraint effect. International Journal of Plasticity. 2017;89:96-109.https://doi.org/10.1016/j.ijplas.2016.11.005
[9] Yao HB, Ge J, Mao LB, Yan YX, Yu SH. Artificial carbonate nanocrystals and layered structural nanocomposites inspired by nacre: synthesis, fabrication and applications. ChemInform. 2014;45:no-no.https://doi.org/10.1016/j.jallcom.2018.10.357
[10] Firkowska I, Boden A, Boerner B, Reich S. The origin of high thermal conductivity and ultralow thermal expansion in copper–graphite composites. Nano letters. 2015;15:4745-51.https://doi.org/10.1021/acs.nanolett.5b01664
[11] Wang X, Jiang X, Sun H, Zhang Y, Fang Y, Shu R. Microstructure and mechanical properties of bioinspired laminated Al matrix hybrid reinforced with $B_4C$ and graphene nanoplatelets. Materials Characterization. 2022;193:112307.https://doi.org/10.1016/j.matchar.2022.112307
[12] Liang Y, Jiang L, Zhang X, Pei Z, Lei Q. Microstructure, mechanical and tribological properties of Cu-Sn/$Cr_3C_2$/Gr composites. Composite Structures. 2023;324:117575.https://doi.org/10.1016/j.compstruct.2023.117575
[13] Dixit M, Srivastava R. The effect of copper granules on interfacial bonding and properties of the copper-graphite composite prepared by flake powder metallurgy. Advanced Powder Technology. 2019;30:3067-78.https://doi.org/10.1016/j.apt.2019.09.013
[14] Ahmadian H, Sadoun AM, Fathy A, Zhou T. Utilizing a unified conceptual dynamic model for prediction of particle size of duel-matrix nanocomposites during mechanical alloying. Powder Technology. 2023;418.https://doi.org/10.1016/j.powtec.2023.118291
[15] Yoo SC, Lee J, Hong SH. Synergistic outstanding strengthening behavior of graphene/copper nanocomposites. Composites Part B: Engineering. 2019;176:107235.https://doi.org/10.1016/j.compositesb.2019.107235
[16] Wang S, Liu M, Araby S, Wang X, Abdelsalam AA, Xue H, et al. Reinforcing interlaminar interface of carbon fiber reinforced metal laminates by graphene. Composite Structures. 2023;311:116814.https://doi.org/10.1016/j.compstruct.2023.116814
[17] Liu B, Zhang D-q, Li X-f, Guo X-h, Shi J, Liu Z-j, et al. The microstructures and properties of graphite flake/copper composites with high volume fractions of graphite flake. New Carbon Materials. 2020;35:58-65.https://doi.org/10.1016/j.carbon.2020.04.053
[18] Balandin AA, Ghosh S, Bao W, Calizo I, Teweldebrhan D, Miao F, et al. Superior thermal conductivity of single-layer graphene. Nano letters. 2008;8:902-7.https://doi.org/10.1021/nl0731872
[19] Ahmadian H, Zhou T, Abd Elaziz M, Azmi Al-Betar M, Sadoun AM, Najjar IMR, et al. Predicting crystallite size of Mg-Ti-SiC nanocomposites using an adaptive neuro-fuzzy inference system model

modified by termite life cycle optimizer. Alexandria Engineering Journal. 2023;84:285-300.https://doi.org/10.1016/j.aej.2023.11.009
[20] Liu Q, He X-B, Ren S-B, Zhang C, Ting-Ting L, Qu X-H. Thermophysical properties and microstructure of graphite flake/copper composites processed by electroless copper coating. Journal of Alloys and Compounds. 2014;587:255-9.https://doi.org/10.1016/j.jallcom.2013.09.207
[21] Sadoun A, Ibrahim A, Abdallah AW. Fabrication and evaluation of tribological properties of $Al_2O_3$ coated Ag reinforced copper matrix nanocomposite by mechanical alloying. Journal of Asian Ceramic Societies. 2020;8:1228-38.https://doi.org/10.1080/21870764.2020.1841073
[22] Fan G, Jiang Y, Tan Z, Guo Q, Xiong D-b, Su Y, et al. Enhanced interfacial bonding and mechanical properties in CNT/Al composites fabricated by flake powder metallurgy. Carbon. 2018;130:333-9.https://doi.org/10.1016/j.carbon.2018.01.037
[23] Sadoun AM, Meselhy AF, Abdallah AW. Microstructural, mechanical and wear behavior of electroless assisted silver coated $Al_2O_3$–Cu nanocomposites. Materials Chemistry and Physics. 2021;266.https://doi.org/10.1016/j.matchemphys.2021.124562
[24] Kováčik J, Emmer Š, Bielek J, Keleši Lu. Effect of composition on friction coefficient of Cu–graphite composites. Wear. 2008;265:417-21.https://doi.org/10.1016/j.wear.2007.11.012
[25] Luo F, Jiang X, Sun H, Mo D, Zhang Y, Shu R, et al. High thermal and electrical properties of electroless graphene films reinforced Cu matrix laminated composites. Journal of Alloys and Compounds. 2022;925:166710.https://doi.org/10.1016/j.jallcom.2022.166710
[26] Zhao R, Li W, Wang T, Zhan K, Yang Z, Yan Y, et al. Fabrication of Cu/graphite film/Cu sandwich composites with ultrahigh thermal conductivity for thermal management applications. Frontiers of Materials Science. 2020;14:188-97.https://doi.org/10.1007/s11706-020-0503-y
[27] Chu K, Wang X-h, Wang F, Li Y-b, Huang D-j, Liu H, et al. Largely enhanced thermal conductivity of graphene/copper composites with highly aligned graphene network. Carbon. 2018;127:102-12.https://doi.org/10.1016/j.carbon.2017.10.099
[28] Barakat WS, Habba MIA, Ibrahim A, Fathy A, Elkady OA. The effect of Cu coated $Al_2O_3$ particle content and densification methods on the microstructure and mechanical properties of Al matrix composites. Journal of Materials Research and Technology. 2023;24:6908-22.https://doi.org/10.1016/j.jmrt.2023.05.010
[29] Khamaj A, Farouk WM, Shewakh WM, Abu-Oqail AMI, Wagih A, Abu-Okail M. Effect of lattice structure evolution on the thermal and mechanical properties of Cu–$Al_2O_3$/GNPs nanocomposites. Ceramics International. 2021;47:16511-20.https://doi.org/10.1016/j.ceramint.2021.02.219
[30] Sadoun AM, Fathy A, Abu-Oqail A, Elmetwaly HT, Wagih A. Structural, mechanical and tribological properties of Cu–$ZrO_2$/GNPs hybrid nanocomposites. Ceramics International. 2020;46:7586-94.https://doi.org/10.1016/j.ceramint.2019.11.258
[31] Abu-Oqail A, Samir A, Essa ARS, Wagih A, Fathy A. Effect of GNPs coated Ag on microstructure and mechanical properties of Cu-Fe dual-matrix nanocomposite. Journal of Alloys and Compounds. 2019;781:64-74.https://doi.org/10.1016/j.jallcom.2018.12.042
[32] Erb RM, Libanori R, Rothfuchs N, Studart AR. Composites reinforced in three dimensions by using low magnetic fields. Science. 2012;335:199-204.https://doi.org/10.1126/science.1210822
[33] Shen X-Y, He X-B, Ren S-B, Zhang H-M, Qu X-H. Effect of molybdenum as interfacial element on the thermal conductivity of diamond/Cu composites. Journal of Alloys and Compounds. 2012;529:134-9.https://doi.org/10.1016/j.jallcom.2012.03.045

[34] Zhang Y, Sun Z, Zhou Y. Cu/$Ti_3SiC_2$ composite: a new electrofriction material. Materials Research Innovations. 2016;3:80-4.https://doi.org/10.1007/s100190050129
[35] Pasumarthi V, Chen Y, Bakshi SR, Agarwal A. Reaction synthesis of $Ti_3SiC_2$ phase in plasma sprayed coating. Journal of Alloys and Compounds. 2009;484:113-7.https://doi.org/10.1016/j.jallcom.2009.04.079
[36] Zhang R, Liu F, Tulugan K. Self-lubricating behavior caused by tribo-oxidation of $Ti_3SiC_2$/Cu composites in a wide temperature range. Ceramics International. 2022;48:15504-15.https://doi.org/10.1016/j.ceramint.2022.02.084
[37] Shu R, Jiang X, Shao Z, Sun D, Zhu D, Luo Z. Fabrication and mechanical properties of MWCNTs and graphene synergetically reinforced Cu–graphite matrix composites. Powder Technology. 2019;349:59-69. https://doi.org/10.1016/j.powtec.2019.03.021
[38] Dang W, Ren S, Zhou J, Yu Y, Li Z, Wang L. Influence of Cu on the mechanical and tribological properties of $Ti_3SiC_2$. Ceramics International. 2016;42:9972-80.https://doi.org/10.1016/j.ceramint.2016.03.099
[39] Guan C, Zhao Y, Chen G, Kai X, Qian W, Tao R, et al. Synergistic strengthening and toughening of copper coated graphene nanoplates and in situ nanoparticles reinforced AA6111 composites. Materials Science and Engineering: A. 2021;822:141661.https://doi.org/10.1016/j.msea.2021.141661
[40] Melaibari A, Wagih A, Basha M, Kabeel AM, Lubineau G, Eltaher MA. Bio-inspired composite laminate design with improved out-of-plane strength and ductility. Composites Part A: Applied Science and Manufacturing. 2021;144.https://doi.org/10.1016/j.compositesa.2021.106362
[41] Tan W, Jiang X, Shao Z, Sun H, Fang Y, Shu R. Fabrication and mechanical properties of nano-carbon reinforced laminated Cu matrix composites. Powder Technology. 2022;395:377-90.https://doi.org/10.1016/j.powtec.2021.09.072
[42] Ghandourah E, Ahmadian H, Zhou T, Sadoun AM, Fathy A, Atif M, et al. Comprehensive investigation of the impact of milling time on microstructural evolution and tribological properties in Mg-Ti-SiC hybrid composites. Materials Today Communications. 2024;38.https://doi.org/10.1016/j.mtcomm.2023.107835
[43] Ali M, Sadoun AM, Abouelmagd G, Mazen AA, Elmahdy M. Microstructure and mechanical characterization of Cu–Ni/$Al_2O_3$ nanocomposites fabricated using a novel in situ reactive synthesis. Ceramics International. 2022;48:6414-22.https://doi.org/10.1016/j.ceramint.2021.11.185
[44] Najjar IR, Sadoun AM, Fathy A, Abdallah AW, Elaziz MA, Elmahdy M. Prediction of Tribological Properties of Alumina-Coated, Silver-Reinforced Copper Nanocomposites Using Long Short-Term Model Combined with Golden Jackal Optimization. Lubricants. 2022;10.https://doi.org/10.3390/lubricants10110277
[45] Cao M, Xiong D-B, Tan Z, Ji G, Amin-Ahmadi B, Guo Q, et al. Aligning graphene in bulk copper: Nacre-inspired nanolaminated architecture coupled with in-situ processing for enhanced mechanical properties and high electrical conductivity. Carbon. 2017;117:65-74.https://doi.org/10.1016/j.carbon.2017.02.089
[46] Varol T, Canakci A. Microstructure, electrical conductivity and hardness of multilayer graphene/copper nanocomposites synthesized by flake powder metallurgy. Metals and materials international. 2015;21:704-12.https://doi.org/10.1007/s12540-015-5058-6
[47] Tan Z, Li Z, Fan G, Guo Q, Kai X, Ji G, et al. Enhanced thermal conductivity in diamond/aluminum composites with a tungsten interface nanolayer. Materials & Design. 2013;47:160-6.https://doi.org/10.1016/j.matdes.2012.11.061

[48] Zhang Y, Zhang H, Wu J, Wang X. Enhanced thermal conductivity in copper matrix composites reinforced with titanium-coated diamond particles. Scripta Materialia. 2011;65:1097-100.https://doi.org/10.1016/j.scriptamat.2011.09.028
[49] Swartz ET, Pohl RO. Thermal boundary resistance. Reviews of modern physics. 1989;61:605-68.https://doi.org/10.1103/RevModPhys.61.605
[50] Yuan J, Zhang K, Li T, Li X, Li Y, Ma M, et al. Anisotropy of thermal conductivity and mechanical properties in Mg–5Zn–1Mn alloy. Materials & Design. 2012;40:257-61.https://doi.org/10.1016/j.matdes.2012.03.046
[51] Li W, Liu Y, Wu G. Preparation of graphite flakes/Al with preferred orientation and high thermal conductivity by squeeze casting. Carbon. 2015;95:545-51.https://doi.org/10.1016/j.carbon.2015.08.063
[52] Long XJ, Li B, Wang L, Huang JY, Zhu J, Luo SN. Shock response of Cu/graphene nanolayered composites. Carbon. 2016;103:457-63.https://doi.org/10.1016/j.carbon.2016.03.039